Mechatronics 116 (2026) 103470

Contents lists available at ScienceDirect

Mechatronics

journal homepage: www.elsevier.com/locate/mechatronics

Experimental validation of model-based collocated control for shape regulation in elastically decoupled underactuated soft robots☆,☆☆

Ghanishtha Bhatti [a], Pietro Pustina [a], Daniel Feliu-Talegon [a,*], Bastian Deutschmann [b], Cosimo Della Santina [a,b]

[a] Department of Cognitive Robotics, Delft University of Technology, 2628CN Delft, The Netherlands
[b] Institute of Robotics and Mechatronics, German Aerospace Center (DLR), 82234 Oberpfaffenhofen, Germany

ARTICLE INFO

Keywords:
Soft robotics
Model-based control
Experimental validation
Shape regulation

ABSTRACT

Soft robots, with their compliant and underactuated nature, pose significant challenges for real-time shape regulation. Practical implementations of these methods often rely on fully-actuated approximations, over-looking the underactuated nature of these continuum structures. This study experimentally validates model-based controllers through collocated control that explicitly address underactuation, incorporating gravity cancellation and elasticity compensation to outperform conventional PD/PID approaches. A new multi-segment soft robot with a passively actuated segment has been designed, enabling experimental validation and providing strong evidence of the controllers' effectiveness. The work bridges theory and practice, offering a practical framework for real-time shape regulation applicable to diverse soft robotic systems.

1. Introduction

Over the past decade, interest in human–machine interaction and bioinspired robotic systems has fueled major advancements in soft robotics. This specialized category of robotic systems intentionally incorporates compliant elements into their mechanical structure, leveraging their unique properties for enhanced functionality [1,2].

However, the remarkable flexibility of soft robots inherently comes with infinite degrees of freedom, which pose significant challenges for modeling, control, and estimation of their states [3–5]. A significant advancement has been the development of models based on rod models theory, which use geometric representations to discretize the robot's configuration and derive a finite set of ordinary differential equations (ODEs) that are tractable for control [6–8].

Despite substantial progress in materials, design, and modeling techniques, achieving precise and fast regulation of a robot's configuration remains an open control challenge [4]. Simplified models with reduced degrees of freedom have been developed to approximate system behavior, yet soft robots remain inherently underactuated. This underactuation expands their reachable configuration space at comparable actuator cost and energy consumption relative to fully actuated systems [9]. However, it complicates the control of these systems, which hinders the direct application of classical robotic control methods [10].

While data-driven controllers have addressed this challenge by bypassing the need for complex models [11–13], obtaining the large volumes of data required to construct a comprehensive control policy is often impractical. Moreover, their limited ability to generalize to situations not represented in the training set can lead to undesirable or unstable behaviors. These limitations have motivated the development of model-based control strategies, which leverage knowledge of system dynamics to enhance regulation performance. However, implementing such strategies requires a careful trade-off between model accuracy and computational tractability to meet real-time control demands [14]. Recent advances in reduced-order modeling have been pivotal in bridging this gap, enabling the development of robust control methods with proven stability guarantees [15].

Several works, such as [16–20] have employed finite dimensional models for controlling soft robots in both configuration and task space. Most model-based approaches assume fully actuated dynamics, enabling the use of conventional rigid robot control theory. However, such simplifications can misrepresent system stability and degrade performance—critical aspects for robots designed to interact safely with humans. In reality, soft robots are inherently underactuated and highly

☆ This article is part of a Special issue entitled: 'TC 4.3 Robotics (IFAC WC 2026)' published in Mechatronics.

☆☆ The research was financially supported in part by the Dutch Research Foundation (NWO) through the VENI grant ROSES 20297, in part by European Union's Horizon Europe Program, Project EMERGE, under Grant Agreement 101070918 and in part by the European Union (ERC, RIPLEY, 101165078).

* Corresponding author.
E-mail address: d.feliutalegon@tudelft.nl (D. Feliu-Talegon).

https://doi.org/10.1016/j.mechatronics.2026.103470
Received 26 October 2025; Received in revised form 28 January 2026; Accepted 3 February 2026
Available online 18 February 2026

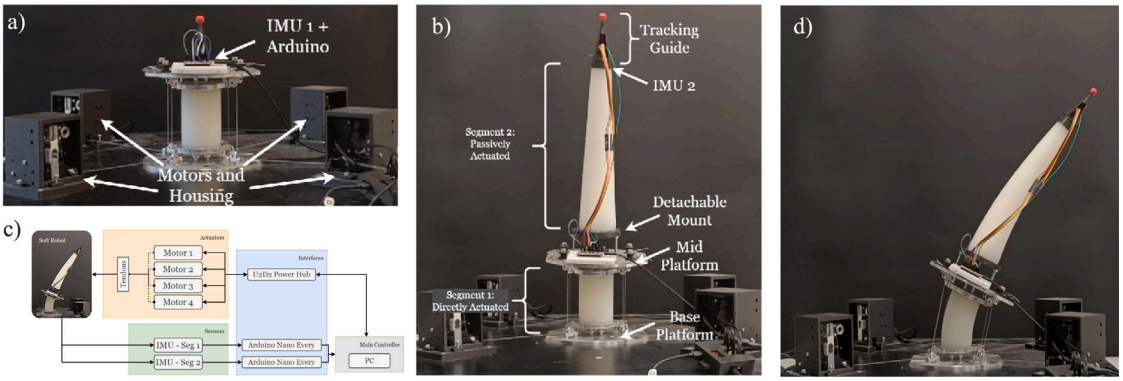

Fig. 1. Mechanical and electronic components of the soft robotic platform: (a) SV1 variant, (b) SV2 variant with a detachable mount between the two segments, allowing switching between the SV1 and SV2 configurations, (c) overview of the hardware and interfaces, and (d) SV2 in a bent configuration resulting from a constant actuation.

nonlinear systems, continuously influenced by elastic and dissipative forces that provide natural stabilization.

Some works that have addressed the challenge of regulating the state of underactuated soft continuum robots to a constant setpoint for specific systems include [21], which combines a stabilizing energy-shaping controller with a robustifying PI-like law, and [22], which uses partial feedback linearization and a passivity-based approach. However, a general approach that applies to a broader class of continuum robots, provides stability guarantees, and works in real-time applications is still missing. To address these challenges, [23,24] exploited both actuated and unactuated degrees of freedom, but relied on constant actuation matrices, limiting generality. Recently, [25] derived conditions for decoupling Lagrangian systems into a collocated form through a change of coordinates, thereby extending the applicability of these constant-matrix techniques to a broader range of soft robots. This advancement validates the previously proposed controllers; however, these studies still lack the experimental validation needed to empirically assess the robustness of the control architecture and to systematically compare different controllers in terms of efficiency, steady-state accuracy, and transient performance. One of the few works using the mentioned collocated form in experiments is [26]. It uses a specific controller with compensation for elastic and gravitational forces to control a particular parallel robot, with the main focus on task-space regulation.

Consequently, this work addresses the gap of exploring the experimental aspects of soft robot control through the implementation of real-time, model-based controllers using the previously mentioned collocated form. For this venue, we purposely developed a novel multi-segment soft robot prototype that enables the separation of actuated and unactuated degrees of freedom. This design allows their explicit inclusion in the feedback control loop, facilitating a more accurate evaluation of control performance. Our objective is to demonstrate on hardware setups that model-based control can significantly enhance shape regulation control performance compared to conventional model-free alternatives. In doing so, we provide empirical evidence of robustness for controllers that incorporate both actuated and unactuated degrees of freedom, advancing the broader understanding of soft robotic control strategies and their applicability across a wide range of robotic platforms.

2. Preliminaries

2.1. Soft robot model

The soft robot model is established using the piecewise constant curvature (PCC) model with an improved state parametrization [8]. Consider a PCC robot composed of n constant-curvature (CC) segments

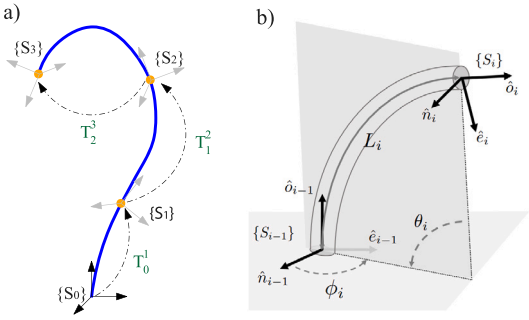

Fig. 2. Kinematic model of a PCC soft robot. Panel (a) illustrates a PCC soft robot composed of three CC segments. (b) details the ith segment.

connected in series, as illustrated in Fig. 2.a. We introduce n reference frames $S_1, \ldots, S_n$, each attached to the end of a segment, along with a fixed base frame S_0. Then, the kinematics configuration of the robot can be given by $q = (\Delta x, \Delta y, \delta L)$. The two curvature coordinates Δx and Δy are related to the angles ϕ and θ of Fig. 2.b and δL represents the length increase with respect to the initial value L_0:

$$\phi(q) = \arccos\left(\frac{\Delta x}{\Delta}\right) = \arcsin\left(\frac{\Delta y}{\Delta}\right), \quad \theta(q) = \Delta, \tag{1}$$

where $\Delta = \sqrt{\Delta x^2 + \Delta y^2}$. The homogeneous transformation matrix T^i_{i-1} of each PCC segment, representing the pose of frame $\{S_i\}$ with respect to the preceding frame $\{S_{i-1}\}$ consists of a rotation part $R^i_{i-1} \in SO(3)$ and a translation part $tr^i_{i-1} \in \mathbb{R}^3$. This transformation matrix is formulated as:

$$T^i_{i-1} = \begin{bmatrix} R^i_{i-1} & tr^i_{i-1} \\ 0_3 & 1 \end{bmatrix}, \qquad tr^i_{i-1} = \frac{(L_0 + \delta L)}{\Delta^2} \begin{bmatrix} \Delta_x(1 - \cos(\frac{\Delta s}{L_0})) \\ \Delta_y(1 - \cos(\frac{\Delta s}{L_0})) \\ \Delta(\sin(\frac{\Delta s}{L_0})) \end{bmatrix}$$

$$R^i_{i-1} = \begin{bmatrix} 1 + \frac{\Delta_x^2}{\Delta^2}\left(\cos\left(\frac{\Delta s}{L_0}\right) - 1\right) & \frac{\Delta_x \Delta_y}{\Delta^2}\left(\cos\left(\frac{\Delta s}{L_0}\right) - 1\right) & \frac{\Delta_x}{\Delta}\sin\left(\frac{\Delta s}{L_0}\right) \\ \frac{\Delta_x \Delta_y}{\Delta^2}\left(\cos\left(\frac{\Delta s}{L_0}\right) - 1\right) & 1 + \frac{\Delta_y^2}{\Delta^2}\left(\cos\left(\frac{\Delta s}{L_0}\right) - 1\right) & \frac{\Delta_y}{\Delta}\sin\left(\frac{\Delta s}{L_0}\right) \\ -\frac{\Delta_x}{\Delta}\sin\left(\frac{\Delta s}{L_0}\right) & -\frac{\Delta_y}{\Delta}\sin\left(\frac{\Delta s}{L_0}\right) & \cos\left(\frac{\Delta s}{L_0}\right) \end{bmatrix},$$

By applying Lagrangian derivations [8], the general dynamic model of the robot can be formulated based on the kinematic model introduced above

$$M(q)\ddot{q} + C(q, \dot{q})\dot{q} + D(q)\dot{q} + G(q) + Kq = \tau(q), \tag{2}$$

where $q \in R^n$ is the vectors of configuration variables and $M(q)$ and $C(q, \dot{q})$ denote the inertia matrix and the Coriolis terms, respectively,

$G(q)$ represents the gravitational force, and D and K correspond to the damping and stiffness forces, respectively. The term τ denotes the generalized actuation force. The dynamic model (2) can be conveniently rewritten by separating the dynamic equations of the actuated $q_a \in R^{n_a}$ and unactuated variables $q_u \in R^{n-n_a}$, such that $q = (q_a, q_u)$. [23] demonstrates that both actuated and unactuated components of q can be incorporated into (2) to derive

$$\begin{bmatrix} M_{aa} & M_{au} \\ M_{ua} & M_{uu} \end{bmatrix} \begin{bmatrix} \ddot{q}_a \\ \ddot{q}_u \end{bmatrix} + \begin{bmatrix} C_{aa} & C_{au} \\ C_{ua} & C_{uu} \end{bmatrix} \begin{bmatrix} \dot{q}_a \\ \dot{q}_u \end{bmatrix} + \begin{bmatrix} G_a \\ G_u \end{bmatrix} + \begin{bmatrix} K_{aa} & 0 \\ 0 & K_{uu} \end{bmatrix} \begin{bmatrix} q_a \\ q_u \end{bmatrix} + \begin{bmatrix} D_{aa} & D_{au} \\ D_{ua} & D_{uu} \end{bmatrix} \begin{bmatrix} \dot{q}_a \\ \dot{q}_u \end{bmatrix} = \begin{bmatrix} \tau \\ 0 \end{bmatrix}. \tag{3}$$

where the input $\tau = [\tau_{\Delta x} \ \tau_{\Delta y} \ \tau_{\delta L}]$ is the generalized forces in the Δ-parametrization framework. No elastic coupling between the elastic forces of the actuated and unactuated parts is considered in the model, allowing it to describe continuum robots that are elastically decoupled.

2.2. Control strategy

The control strategy is designed to achieve shape regulation, that is, to drive the system toward a desired configuration. The problem can be formulated as follow:

$$\lim_{t\to\infty} q(t) = \bar{q}. \tag{4}$$

where q is the variables to be regulated. Different controllers can be implemented within the model (3), ensuring stability and convergence to the desired shapes.

PD+ Controllers:

$$\tau_1 = K_P(q_a^* - q_a) - K_D\dot{q}_a + G_a(q) + K_{aa}q_a^*. \tag{5}$$

P-SatI-D Controllers:

$$\tau_2 = K_P(q_a^* - q_a) - K_D\dot{q}_a + K_I \int_0^t s(q_a^* - q_a(\rho))d\rho + G_a(q) + K_{aa}q_a^* \tag{6}$$

where for the purposes of experimental verification, two saturation functions $s(y)$ are chosen: ($s_t(y) = \tanh y$) and ($s_p(y) = \frac{y}{(1+|y|^p)^{\frac{1}{p}}}$) where $p \in \mathbb{Z}^+$.

Theorem 1 ([23]). *Suppose the robot is elastically decoupled (3). If K_P is large enough, the trajectories of the closed-loop system (3) together with the control law (5), are bounded and converge asymptotically to the equilibrium state $(q_a, q_u, \dot{q}_a, \dot{q}_u) = (q_a^*, \bar{q}_u, 0, 0)$, where $\bar{q}_u$ is a solution of the equilibrium equation*

$$K_{uu}q_u + G_u(q_a^*, q_u) = 0 \tag{7}$$

.

Theorem 2 ([24]). *For an elastically decoupled soft robot (3)$\alpha_P > 0$ and $K_I > 0$, such that for all $K_P > \alpha_P I_m$, the trajectories of the closed-loop system (3) together with the control law (6), are bounded and converge asymptotically to the equilibrium state $(q_a, q_u, \dot{q}_a, \dot{q}_u) = (q_a^*, \bar{q}_u, 0, 0)$, where $\bar{q}_u$ is a solution of the equilibrium Eq. (7).*

In shape regulation, incorporating a system model can significantly enhance the performance of PD/PID-style controllers. For this reason, we propose to use a third controller, which does not offer theoretical guarantees, but corresponds to a PID controller with gravity compensation and elasticity cancellation, similar to controllers (5) and (6).

PID+ Controllers:

$$\tau_3 = K_P(q_a^* - q_a) - K_D\dot{q}_a + K_I \int_0^t \left[q_a^* - q_a(\rho)\right] d\rho + G_a(q) + K_{aa}q_a^*. \tag{8}$$

2.3. Zero dynamics stability

Considering the model (3), and assuming that the actuated variables q_a are regulated to a constant value q_a^* using one of the proposed controllers, the presence of the unactuated dynamics implies that the system exhibits a zero dynamics of dimension $2(n - n_a)$. This can be easily derived by examining the residual dynamics in (3) when $\dot{q}_a$ and $\ddot{q}_a$ are set to zero

$$M_{uu}(q_a^*, q_u)\ddot{q}_u + C_{uu}(q_a^*, q_u, 0, \dot{q}_u)\dot{q}_u + G_u(q_a^*, q_u) + K_{uu}q_u + D_{uu}(q_a^*, q_u)\dot{q}_u = 0. \tag{9}$$

Lemma 1. *For any initial state, the trajectories of (9) are bounded and converge to $(q_u, \dot{q}_u) = (\bar{q}_u, 0)$, where $\bar{q}_u$ is a solution of the equilibrium Eq. (7).*

Proof. Consider the Lyapunov-like function

$$V(q_u, \dot{q}_u) = \frac{1}{2}\dot{q}_u^T M_{uu}(q_a^*, q_u)\dot{q}_u + \frac{1}{2}q_u^T K_{uu}q_u + U(q_a^*, q_u) \tag{10}$$

The gravitational potential $U(q_a^*, q_u)$ is lower bounded, which implies that $V(q_u, \dot{q}_u)$ is also lower bounded. We then evaluate $\dot{V}$ along the trajectories of (9), obtaining $\dot{V} = -\dot{q}_u^T D_{uu}\dot{q}_u \leq 0$. Since V is both radially unbounded and lower bounded, it is possible to invoke the corollary to LaSalle's invariance principle [27], thus concluding the proof. The equilibrium (7) reached by the unactuated variables is not unique in general, the sufficient condition for the uniqueness of $\bar{q}_u$ is provided in the following corollary.

Corollary 1. *Under the hypothesis that trajectories of the closed-loop system (3) converges asymptotically to (7), if*

$$K_{uu} > \frac{\delta^2 U(q_a^*, \bar{q}_u)}{\delta q_u^2} \tag{11}$$

for all $q_u \in \mathbb{R}^{n-n_a}$, then the solution (7) is a unique globally asymptotically stable equilibrium.

Proof. Consider the Lyapunov-like function

$$P(q_u) = U(q_a^*, \bar{q}_u) + \frac{1}{2}q_u^T K_{uu}q_u \tag{12}$$

According to Theorems 1 and 2, the unactuated variables converge to a value $\bar{q}_u$ satisfying $G_u(q_a^*, \bar{q}_u) + K_{uu}\bar{q}_u = 0$. This expression corresponds to the gradient of $P(q_u)$ evaluated at the closed-loop equilibrium, implying that $\bar{q}_u$ is an extremum of $P(q_u)$. Moreover, this equilibrium point is unique, since the Hessian of $P(q_u)$ given by $\delta^2 U(q_a^*, \bar{q}_u)/\delta q_u^2 + K_{uu}$, is positive definite by hypothesis.

3. Soft robot platform design

We developed a modular soft robot platform inspired by the mechanical design presented in [28]. This design consists of a continuously deformable structure placed between two rigid platforms. An additional soft segment is attached above the upper platform via a detachable mount, resulting in a versatile configuration that can operate as either a single-segment (SV1) or a two-segment (SV2) system (see Fig. 1). This novel design allows us to introduce a passive component into the system, further emphasizing the inherently underactuated nature of the platform, and to investigate how the controllers deal with both the actuated and underactuated components.

In this platform, four actuated tendons are routed from the lower to the upper platform, such that the first segment (S1) is actively controlled while the second segment (S2) remains passive and is indirectly actuated through the middle platform movement. The tendons are guided by rotatable pulleys equipped with bearings to reduce friction during tendon motion. The metallic components of the platform are machined from aluminum to withstand large forces without deformation or deterioration, while the soft bodies consist of two silicone segments

Table 1
Parameters of Soft Robot Segments.

Parameter	Units	S1	S2
Mass*	kg	0.543	0.639
Length*	m	0.095	0.3
Radius*	m	0.0325	0.0325
Young's Modulus^{id}	Pa	3.67×10^5	2.01×10^5
Poisson's Ratio^{m}	–	0.3	0.3
Damping Coefficient^{id}	Ns/m	0.854	0.191

(*) measured, (^{id}) identified, (^{m}) manufacturer specification

fabricated through a mold-casting process using Dragon Skin 30 A. Moreover, a 3D-printed cone was placed at the tip of the prototypes to serve as a visual marker during the experiments.

Actuation is achieved through the system's tendons. Each tendon is driven by a dedicated Dynamixel® XH430-W350 servo motor, connected in a daisy-chain via a U2D2 power hub for centralized serial communication. Custom software wrappers built on the Dynamixel® SDK enable synchronous current commands to the four motors, based on the control actions computed by the controller.

The robot is also equipped with two Adafruit® BNO055 IMU sensors, one at the endpoint of each soft segment, to measure their orientations and derive segment curvature in both the x and y directions. Tendon length variations are measured using motor encoders instead of IMU data to minimize noise, allowing elongation and compression estimation only for S1. For S2, these effects are assumed negligible due to its material properties and the absence of tendons in this segment. An overview of the hardware interfaces is presented in Fig. 1.

4. Simulations and experiments results

In this section, the proposed controllers are tested both in simulation and on the soft robot prototype described in Section 2. We also compare their performance with model-free PD and PID controllers, similar to (5), (6) and (8), but excluding the gravitational and elastic terms. The model free PD/PID controllers considered here are not plain PD/PID schemes, as they regulate the robot shape through actuated coordinates, $q_a = (\Delta x_{S1}, \Delta y_{S1}, \delta L_{S1})$ defined in the model, rather than directly controlling joint variables, which would correspond to servo-level control of the tendon-driven motors. The references for these actuated coordinates are computed from the desired shape, defined to achieve a task-space objective such as positioning the robot tip. The physical actuations are the tendon lengths, which are mapped to these actuated coordinates in order to implement the proposed controller. Controller gains are tuned using a Ziegler–Nichols–inspired procedure, first reducing steady-state error and then minimizing settling time. In this study, we experimentally evaluate six controllers—two model-free and four state-of-the-art model-based controllers with stability guarantees—to compare their performance. The goal is to analyze how model-based components influence the transient response of the system, and how integral and derivative actions affect steady-state error and transient behavior in these complex systems.

4.1. Simulation results

Using the model parameters detailed in Table 1, we have simulated the behavior of the robot in both SV1 and SV2 variants. Each body is modeled as a single PCC segment. For the SV1 variant, all the degrees of freedom considered by the PCC kinematic formulation are actuated $q = q_a = (\Delta x_{S1}, \Delta y_{S1}, \delta L_{S1})$, leading to the model (3) but including only the actuated part. In the case of the SV2 variant, the kinematics of S2 are also considered; these are unactuated based on the robot design. Thus, $q = (q_a, q_u) = (\Delta x_{S1}, \Delta y_{S1}, \delta L_{S1}, \Delta x_{S2}, \Delta y_{S2}, \delta L_{S2})$, leading to the elastically decoupled model (3). For the purposes of this paper, we opted to model both segments using a single PCC as a compromise between accuracy and simplicity. The first segment is sufficiently short to be accurately approximated with a single PCC element. The second segment can also be modeled with a single PCC because, despite being quite long and influenced by gravity, the initial configuration of the system is oriented upwards, and the segment has a conical shape that reduces the effect of gravity toward the tip. Under these conditions, the resulting deformation can be accurately approximated using a single PCC element.

The controllers mentioned in the previous Section were implemented in our simulator yielding the results shown in Tables 2 and 3. The simulation results demonstrate perfect setpoint regulation with zero steady-state error for all controllers except the PD, which has a very small errors expected from testing on an ideal model with no uncertainty. The PD and PD+ require significantly higher proportional gains to achieve their best possible performance. Comparing segment performances in the SV2 variant, S2 consistently exhibits slower settling than S1, with an average difference of 0.3595 s attributed to the inertia of the passively actuated S2.

4.2. Experimental results

To thoroughly assess the controller performance, the system was tested under a wide range of experimental conditions. The sensory and actuation systems are fully embedded in the platform, while a motion tracking system is used to evaluate the accuracy of the approach and provide the ground truth. The resultant generalized force τ, generated by the tension of the four tendons actuating the soft platform, was computed as

$$\begin{bmatrix} \tau_{\Delta x} \\ \tau_{\Delta y} \\ \tau_{\delta L} \end{bmatrix} = \begin{bmatrix} d & d & -d & -d \\ d & -d & d & -d \\ 1 & 1 & 1 & 1 \end{bmatrix} \begin{bmatrix} F_1 \\ F_2 \\ F_3 \\ F_4 \end{bmatrix}. \tag{13}$$

Here, d denotes the distance between the center of the platform and the point where each force is applied. The problem is formulated as an optimization task, with the constraint $F_m = \{F_1, F_2, F_3, F_4\} \in \mathbb{R}^+$, since negative tendon forces are physically equivalent to zero.

The experimental results from SV1 and SV2 tested using the different controllers are given in Fig. 3, Tables 4 and 5. Fig. 3 presents the response of only the Δx component of both the actuated and unactuated parts, as similar behavior was observed for the remaining components. Simulations show an average settling time that is 61.6% shorter than in the experiments using SV1. The difference arises because the model does not account for the motor's velocity limit (32 rpm), which constrains the achievable settling time in hardware.

On the SV1 variant, the PID+ controller achieves the lowest steady-state error (0.21%) but with the slowest settling time, while the PD+ controller settles 1.066 s faster at the cost of higher error (3.5%). The baseline PD controller's high gains cause overshoots, lengthening settling time by 35.8%. Adding an integral term in the PID controller reduces both settling time and error, but without model-based terms, its tracking performance remains inferior to PID+.

Compared to SV1, SV2 exhibits an average 28.21% longer settling time, primarily due to its lower damping, which leads to oscillations under sudden accelerations and decelerations. Although passive dynamics inherently decrease accuracy, model-based controllers consistently maintain steady-state errors below 10%, validating their robustness. Notably, regulation accuracy in S1 shows how PID controllers and PD+ reduce the error considerably. We can see that the error in S2 does not follow the same pattern, because the unactuated coordinates associated with the second segment are not directly controlled. They converge to the desired equilibrium values, which depend solely on the model accuracy and do not always translate proportionally to the error of the actuated components.

Table 2
Simulation results for SV1 variant.

Controller	K_P	K_D	K_I	p	Steady State Error (%)	Settling Time (s)	Overshoot (%)	Peak Time (s)
PD	32	3	0	–	0.0563	0.73	0	0.73
PID	16	2	11	–	0	1.085	0.323	1.08
PD+	21	1	0	–	0	0.569	0	0.569
PID+	15	0.5	10	–	0	1.33	0	1.33
P-SatI-D st	15	1	11	–	0	1.195	0.156	0.846
P-SatI-D sp	15	1	11	2	0	1.07	0.148	0.977

Table 3
Simulation results for SV2 variant.

Controller	K_P	K_D	K_I	p	Steady State Error (%)		Settling Time (s)		Overshoot (%)		Peak Time (s)	
					S1	S2	S1	S2	S1	S2	S1	S2
PD	52	3	0	–	0.0534	0.0601	0.474	0.89	0	11.4	0.474	0.52
PID	15	1	7	–	0	0	0.635	1.019	1.02	15.3	0.576	0.587
PD+	47	2	0	–	0	0	0.538	1.011	0	13.11	0.538	0.4905
PID+	10	1	5	–	0	0	0.826	1.13	0	7.5	0.826	0.689
P-SatI-D s_t	15	1	6	–	0	0	0.935	1.271	0	0	0.935	1.271
P-SatI-D s_p	15	1	6	2	0	0	0.897	1.141	0	0	0.897	1.141

Table 4
Experimental results SV1 variant.

Controllers	K_P	K_D	K_I	p	Steady State Error (%)	Settling Time (s)	Overshoot (%)	Peak Time (s)
PD	9.5	0.6	0	–	−3.83	2.94	4.68	1.74
PID	4.8	0.3	0.9	–	−2.05	2.73	3.85	1.98
PD+	1.5	0.6	0	–	−3.50	2.16	0	2.16
PID+	0.56	0.4	0.2	–	0.21	2.97	0.22	2.96
P-SatI-D s_t	0.75	0.4	0.2	–	1.27	2.67	1.27	2.67
P-SatI-D s_p	0.75	0.4	0.3	2	1.24	2.56	0.24	2.56

Table 5
Experimental results SV2 variant.

Controllers	Kp	Kd	Ki	p	Steady State Error (%)		Settling Time (s)		Overshoot (%)		Peak Time (s)	
					S1	S2	S1	S2	S1	S2	S1	S2
PD	2.4	0.5	0	–	−3.31	−1.08	2.52	3.95	0.8	2	1.84	1.9
PID	2.15	0.5	0.2	–	−1.74	−4.85	2.09	3.17	1.2	9.3	2.09	2.4
PD+	0.57	0.1	0	–	0.47	4.71	2.19	3.09	0.47	7.01	2.19	2.07
PID+	0.7	0.2	0.2	–	0.11	3.99	2.84	2.98	0.11	3.99	2.84	2.98
P-SatI-D st	1.1	0.3	0.5	–	1.27	4.55	2.66	3.65	1.27	4.55	2.66	3.65
P-SatI-D sp	0.55	0.2	0.5	2	1.62	6.73	3.34	3.08	1.62	6.88	3.34	2.91

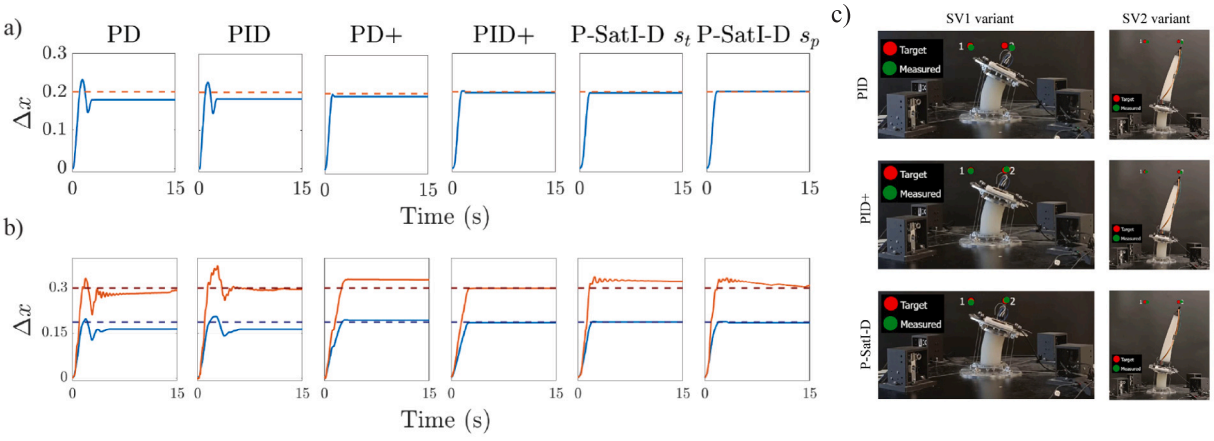

Fig. 3. Experimental results. (a) show Δx_{S1} for multiple shapes in SV1 variant, (b) show Δx_{S1} (blue) and Δx_{S2} (red) for multiple shapes in SV2 variant. The errors observed in the collocated coordinates (blue lines) using the PID-type controllers are nonzero because the system relies on IMU-based orientation measurements, which are not perfectly accurate, whereas the ground truth is obtained from an accurate motion tracking system and (c) steady-state accuracy comparison of controllers, with desired points shown in red and measured points in green.

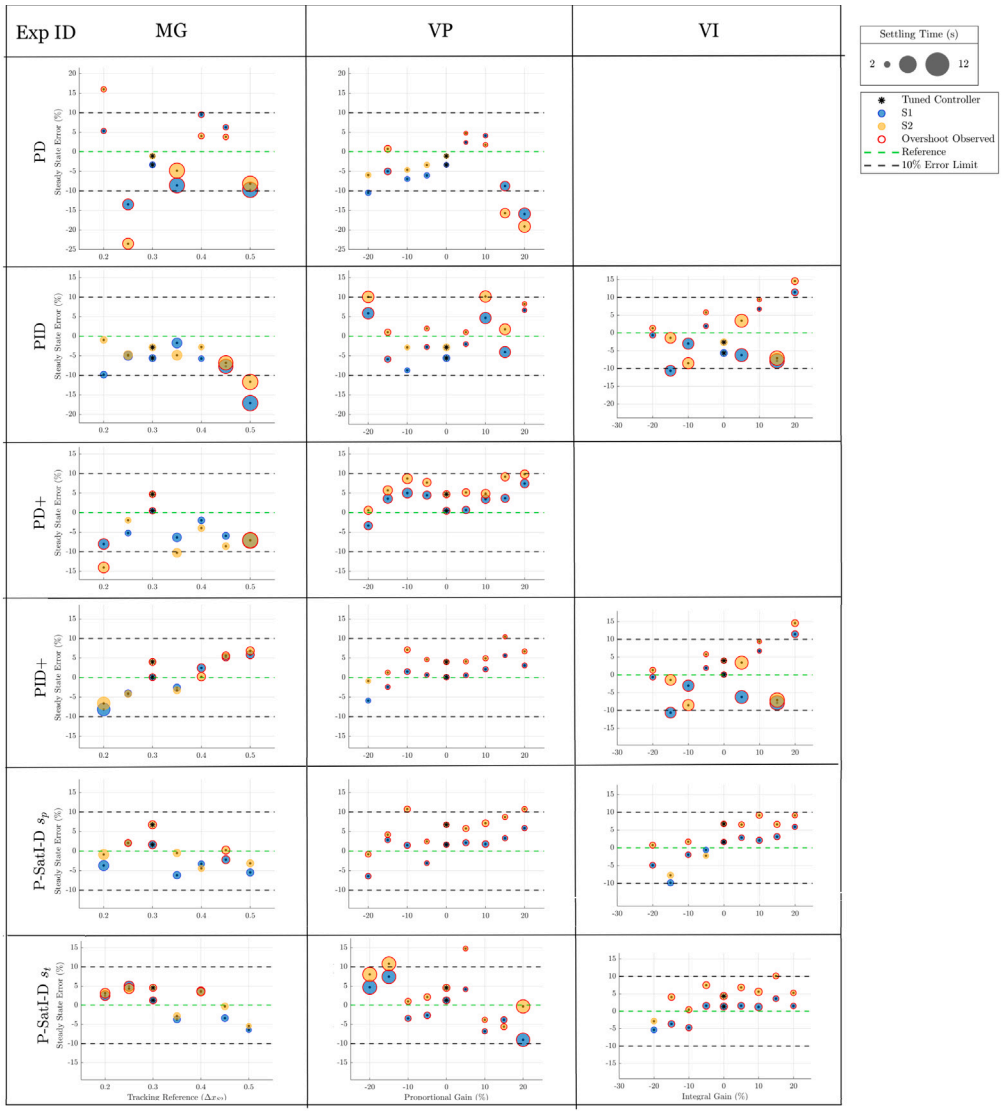

Fig. 4. Robustness analysis. Errors in the actuated (S1) and unactuated (S2) coordinates are shown in blue and yellow, respectively. For each controller, the nominal (tuned) controller is marked with a (*) in the figure. The steady-state error is reported on the y-axis, while the settling time is represented by the radius of the circular marker, which is proportional to its value, and overshoot is indicated by a red outline around the marker (see the figure legend). Moreover, in each column, the x-axis corresponds to a different parameter being varied in order to assess robustness.

4.3. Robustness analysis of the controllers

The robustness of the controllers was evaluated through sequential tracking of multiple 3D shapes, reference variations without retuning, and systematic changes in proportional and integral gains. These experiments were performed on SV2 variant (see Fig. 4).

MG: Shape regulation goal variation

This experiment evaluates the controller's robustness to variations in shape regulation goals without requiring retuning. The controllers were initially tuned to track the configuration $q_a^* = (0.2, 0, 0)$ and $q_u^* = (0.3, 0, 0)$.

Results are shown in the first column of Fig. 4. Analysis of the baseline PD and PID controllers highlights their sensitivity to reference changes: tracking accuracy drops significantly, with the PID controller in particular suffering from overshoot, long settling times, and steady-state errors exceeding 10%.

The PD+ controller performs better than the baseline model-free schemes, but overshoots at workspace extremes still cause slow convergence and large errors. The PID+ controller follows a similar trend, yet its tracking error consistently remains within 10%. In contrast, both variants of the P-SatI-D controller demonstrate strong robustness to reference variations. Even at the most challenging test points, configuration tracking error stays below 8% with acceptable settling times. These results highlight the adaptability and stability of the P-SatI-D controller, underscoring its suitability for scenarios involving dynamic changes in shape regulation goals.

VP: Proportional gain variation

The controller's performance was also evaluated by varying K_p from −20% to +20% around its tuned value. The results can be observed in the second column of Fig. 4. Among the controllers under examination, the PD+ controller demonstrates notable robustness to variations in proportional gain, being the only one to maintain steady state errors consistently within the 10% threshold. However, it can be noted that variations in the proportional gain have a strong negative impact on the settling time in the PD+ controller. Conversely, both the PID+ and P-SatI-D s_p controllers exhibit consistently low settling times. Nonetheless, very high proportional gains cause the steady-state error to go beyond 10%.

VI: Integral gain variation

In this experiment, the controller's performance is evaluated under variations of the integral gain within a range of −20% to 20% of the tuned K_i, with the baseline set at 0%. The experimental results can be observed in third column of Fig. 4.

The P-SatI-D controllers consistently outperform the PID and PID+ controllers in both speed and accuracy. Quantitatively, the $P-SatI-D_{st}$ controller achieves a 59.62% reduction in average settling time across all integral gain variations compared to PID and PID+. Regarding accuracy, even at the largest gain variation, the worst steady-state error for the $P-SatI-D_{sp}$ controller remains below 9.14%, whereas both PID and PID+ exceed the 10% error threshold under a +20% variation.

5. Conclusion

This study demonstrates the effectiveness of model-based controllers for regulating the shape of soft robots through collocated control, validating their theoretical foundations in real-world scenarios. We also present a custom-designed soft robot platform that enables implementing and testing controllers that exploit both actuated and unactuated degrees of freedom, thus addressing the robot's inherently underactuated nature. This platform is not only effective for testing dynamic control strategies for underactuated soft manipulators but also serves as a versatile tool for exploring a variety of control tasks. Its modularity, adaptability to both single- and multi-segment configurations, and ability to incorporate passive components make it suitable for testing strategies related to soft robotics, such as task-space regulation or tracking, with an emphasis on the influence of underactuation on positioning errors and vibration cancellation, compliant actuators, and even hybrid systems involving both rigid and soft elements.

The control strategy employs reduced-order modeling, collocated formulations and explicit model-based controllers to achieve real-time performance without sacrificing accuracy. We further evaluate PD and PID controllers, both with and without model-based components, to quantify the performance improvements introduced by model-based control. Incorporating model-based terms allows our controllers to achieve the control objectives with smaller gains, leading to less aggressive control actions and improved transient responses.

While this approach may yield ideal performance in simulation, applying it to real hardware inevitably introduces mismatches between the physical system and its model. To mitigate this divergence, we demonstrate that a compensatory integral term can be incorporated into the controller, enhancing precision in reference tracking and reducing the steady-state error.

The system assumes ideal motor behavior and uses low-resolution motors, limiting control precision; improved motor control or higher-resolution actuators could enhance performance. IMU drift also introduces steady-state errors, which could be mitigated by integrating higher-resolution absolute sensing.

CRediT authorship contribution statement

Ghanishtha Bhatti: Writing – review & editing, Writing – original draft, Visualization, Validation, Software, Resources, Methodology, Investigation, Data curation, Conceptualization. **Pietro Pustina:** Writing – original draft, Supervision, Investigation, Formal analysis, Conceptualization. **Daniel Feliu-Talegon:** Writing – review & editing, Writing – original draft, Investigation, Conceptualization. **Bastian Deutschmann:** Supervision, Software, Resources. **Cosimo Della Santina:** Writing – review & editing, Project administration, Methodology, Investigation, Funding acquisition, Formal analysis, Conceptualization.

Declaration of competing interest

The authors declare the following financial interests/personal relationships which may be considered as potential competing interests: Daniel Feliu Talegon reports financial support was provided by NWO. If there are other authors, they declare that they have no known competing financial interests or personal relationships that could have appeared to influence the work reported in this paper.

Data availability

Data will be made available on request.

References

[1] Rus D, Tolley MT. Design, fabrication and control of soft robots. Nature 2015;521(7553):467–75.
[2] Runciman M, Darzi A, Mylonas GP. Soft robotics in minimally invasive surgery. Soft Robot 2019;6(4):423–43.
[3] Armanini C, Boyer F, Mathew AT, Duriez C, Renda F. Soft robots modeling: A structured overview. IEEE Trans Robot 2021;39(3):1728–48.
[4] Della Santina C, Duriez C, Rus D. Model-based control of soft robots: A survey of the state of the art and open challenges. IEEE Control Syst Mag 2023;43(3):30–65.
[5] Feliu-Talegon D, Mathew AT, Alkayas AY, Adamu YA, Renda F. Dynamic shape estimation of tendon-driven soft manipulators via actuation readings. IEEE Robot Autom Lett 2024.
[6] Webster III RJ, Jones BA. Design and kinematic modeling of constant curvature continuum robots: A review. Int J Robot Res 2010;29(13):1661–83.
[7] Mathew AT, Feliu-Talegon D, Alkayas AY, Boyer F, Renda F. Reduced order modeling of hybrid soft-rigid robots using global, local, and state-dependent strain parameterization. Int J Robot Res 2025;44(1):129–54.
[8] Della Santina C, Bicchi A, Rus D. On an improved state parametrization for soft robots with piecewise constant curvature and its use in model based control. IEEE Robot Autom Lett 2020;5(2):1001–8.
[9] He B, Wang S, Liu Y. Underactuated robotics: A review. Int J Adv Robot Syst 2019;16(4):1729881419862164.
[10] Keppler M, Ott C, Albu-Schäffer A. From underactuation to quasi-full actuation: Aiming at a unifying control framework for articulated soft robots. Int J Robust Nonlinear Control 2022;32(9):5453–84.
[11] Wang X, Li Y, Kwok KW. A survey for machine learning-based control of continuum robots. Front Robot AI 2021;8:730330.
[12] Chen Z, et al. Data-driven methods applied to soft robot modeling and control: A review. IEEE Trans Autom Sci Eng 2024;22:2241–56.
[13] Bruder D, Fu X, Gillespie RB, Remy CD, Vasudevan R. Data-driven control of soft robots using Koopman operator theory. IEEE Trans Robot 2020;37(3):948–61.
[14] Bruder D, Remy CD, Vasudevan R. Nonlinear system identification of soft robot dynamics using Koopman operator theory. In: 2019 int. conf. robot. automat. 2019, p. 6244–50.
[15] Katzschmann RK, Santina CD, Toshimitsu Y, Bicchi A, Rus D. Dynamic motion control of multi-segment soft robots using piecewise constant curvature matched with an augmented rigid body model. In: 2019 IEEE int. conf. soft robot. 2019, p. 454–61.
[16] Caasenbrood B, Pogromsky A, Nijmeijer H. Control-oriented models for hyperelastic soft robots through differential geometry of curves. Soft Robot 2023;10(1):129–48.
[17] Franco E, Ayatullah T, Sugiharto A, Garriga-Casanovas A, Virdyawan V. Nonlinear energy-based control of soft continuum pneumatic manipulators. Nonlinear Dynam 2021;106(1):229–53.
[18] Caasenbrood B, Pogromsky A, Nijmeijer H. Energy-shaping controllers for soft robot manipulators through port-hamiltonian cosserat models. SN Comput Sci 2022;3(6):494.
[19] Mishra MK, Chakraborty G, Samantaray AK. Trajectory tracking control of a pneumatically actuated continuum manipulator in the presence of obstacles by using terminal sliding mode control. ISA Trans 2023;143:79–93.
[20] Renda F, Mathew A, Talegon DF. Dynamics and control of soft robots with implicit strain parametrization. IEEE Robot Autom Lett 2024;9(3):2782–9.
[21] Soleti G, Massenio PR, Kunze J, Rizzello G. Model-based robust position control of an underactuated dielectric elastomer soft robot. IEEE Trans Robot 2025.
[22] Deutschmann B, Dietrich A, Ott C. Position control of an underactuated continuum mechanism using a reduced nonlinear model. In: 2017 IEEE 56th annual conference on decision and control. IEEE; 2017, p. 5223–30.

[23] Pustina P, Santina CD, De Luca A. Feedback regulation of elastically decoupled underactuated soft robots. IEEE Robot Autom Lett 2022;7(2):4512–9. http://dx.doi.org/10.1109/LRA.2022.3150829.

[24] Pustina P, Borja P, Santina CD, De Luca A. P-satI-D shape regulation of soft robots. IEEE Robot Autom Lett 2023;8(1):1–8.

[25] Pustina P, Della Santina C, Boyer F, De Luca A, Renda F. Input decoupling of lagrangian systems via coordinate transformation: General characterization and its application to soft robotics. IEEE Trans Robot 2024;40:2098–110.

[26] Stölzle M, Rus D, Della Santina C. An experimental study of model-based control for planar handed shearing auxetics robots. In: International symposium on experimental robotics. Springer; 2023, p. 153–67.

[27] Khalil HK, Grizzle JW. In: Nonlinear systems, vol. 3, Prentice hall Upper Saddle River, NJ; 2002.

[28] Deutschmann B, Reinecke J, Dietrich A. Open source tendon-driven continuum mechanism: A platform for research in soft robotics. In: 2022 IEEE int. conf. soft robot.. 2022, p. 54–61.